Nuclear Engineering and Technology 57 (2025) 103855

Contents lists available at ScienceDirect

Nuclear Engineering and Technology

journal homepage: www.elsevier.com/locate/net

Original Article

Dose assessment in several accidental scenarios involving lithium leakage in three IFMIF-DONES lithium system rooms

J. Javier Martínez-Serrano [a,*], Jorge Maestre [b], Yuefeng Qiu [c], Francesco Saverio Nitti [d]

[a] Departamento de Física Aplicada I, Universidad de Málaga, Málaga, Spain
[b] Consorcio IFMIF-DONES España, Granada, Spain
[c] Karlsruhe Institute of Technology, KIT, Karlsruhe, Germany
[d] ENEA Brasimone, Camugnano, BO, I-40032, Italy

ARTICLE INFO

Keywords:
IFMIF-DONES
Gamma dose
Activated corrosion products
Lithium system
Lithium leakage

ABSTRACT

This study assesses the radiological risks from potential failures in the lithium system of the IFMIF-DONES (International Fusion Materials Irradiation Facility - Demo Oriented NEutron Source) facility, focusing on critical components in the Lithium Loop Cell (LLC), Hot Trap (H-trap), and Cold Trap (C-trap) rooms. Seven lithium leak scenarios were analyzed: four in the LLC room (near the electromagnetic pump, Target Lithium TLIC inlet/outlet, and primary heat exchanger), one in the H-trap, and one in the C-trap. Lithium release volumes varied from 0.017 m^3 to 3.8 m^3. Ambient dose equivalent rates, H*(10), were calculated using the MCNP 5.1.40 radiation transport code for gamma-emitting radionuclides like ^{7}Be and activation products. Simulations included structural features affecting gamma transport, and dose maps were generated at various heights and distances from leaks. The most severe radiological conditions arose from the Primary Heat Exchanger (PHX) rupture and C-trap leakage, with peak H*(10) rates of 94 mSv/h and 130 mSv/h, respectively. To meet annual dose limits (50 mSv/year), maximum allowable human intervention times ranged from 32 min (PHX rupture) to 714 min (H-trap failure). Post-leak access to the C-trap room is prohibited due to exceeding red zone thresholds. These results are essential for safety planning, remote handling, and accident mitigation strategies within the IFMIF-DONES lithium loop systems.

1. Introduction

In IFMIF-DONES (International Fusion Materials Irradiation Facility - Demo Oriented NEutron Source) [1], nuclear stripping reactions will occur in the Target System where an accelerated deuteron beam of 40 MeV and 125 mA will collide with a 25 mm thick liquid lithium target jet flowing at a nominal speed of around 15 m/s. These nuclear reactions aim to produce a neutron flux on the order of 1–5 $\times$ 10^{14} n/cm^2/s, which will irradiate a set of material samples causing significant damage. The nuclear reactions aim to be sustained continuously over sufficiently long periods and with a neutron spectrum similar to that expected in the first wall of a future fusion reactor.

In addition to the generation of radioactive hydrogen isotopes, a radiological problem of concern is the presence of activation products within the lithium loop. One such product is ^{7}Be. A high amount of ^{7}Be ($T_{1/2} = 53.3$ d) is generated in d-Li interactions, mainly by the reactions ^{6}Li(d,n)^{7}Be (14.5 %) and ^{7}Li(d,2n)^{7}Be (83.1 %). A small quantity of the beta emitter ^{10}Be ($T_{1/2} = 1.6 \times 10^6$ y) is also produced. ^{7}Be decays in ^{7}Li with the emission of 0.48 MeV gamma radiation. The production rate equilibrium value is around 150 mg, corresponding to 1.89×10^{15} Bq in 345 days of full operation. The plant stops 20 days a year for planned maintenance.

Furthermore, Activated Corrosion Products (ACP) are produced and incorporated into the liquid lithium. These radionuclides result from the activation of metal impurities transported by liquid lithium as they move through the deuteron beam in the target section. Although most of

* Corresponding author.
E-mail address: jmserrano@uma.es (J.J. Martínez-Serrano).

https://doi.org/10.1016/j.net.2025.103855
Received 29 April 2025; Received in revised form 22 July 2025; Accepted 13 August 2025
Available online 21 August 2025

the impurities are trapped and confined by the Impurity Control System (ICS), a small portion remains in the liquid lithium and may be transported along the lithium loop and deposited on the different components due to particular flow conditions. Managing and controlling these activated impurities is essential for ensuring the safety and reliable operation of the facility.

Lithium is a very reactive element, and may produce an exothermic reaction upon contact with air or concrete due to the reaction with the water. For this reason, the lithium rooms are fitted with stainless-steel liners to prevent Li from contacting concrete and to allow for inert atmosphere control. From a safety point of view, several reference accidental scenarios have been identified and postulated for IFMIF-DONES [2], some of them involving the potential failure of lithium (Li) equipment and subsequent Li leakage. These rooms are also equipped with a Li recovery subsystem, which includes catch panels installed beneath critical components of the Li system, designed to capture potential leaks in case of failure and to promote rapid lithium solidification. Additionally, it sectorizes the leakage, reducing the Li exposure area to the room atmosphere.

The main objective of this study is to assess the radiological risk in case of failure of several components of the lithium system and potential leaks at critical points in three rooms of the IFMIF DONES facility: the Lithium Loop Cell (LLC) room, the Hot Trap (H-trap) room, and the Cold Trap (C-trap) room.

2. Li system room components and Li recovery system description

The Lithium Systems area is located on the lower floor of the IFMIF-DONES building (Fig. 1), directly beneath the Test Cell containing the Target System where the lithium liquid target is generated. The systems are distributed into four rooms (Fig. 2a and b): the LLC room, the C-Trap room, the H-trap room, and the Lithium Sampling Cell room.

The LLC houses the Primary Lithium Loop (PLO), which supplies lithium to the Target System after conditioning. Its main components include the Electromagnetic Pump (EMP), capable of circulating 97.5 L/s of liquid lithium (under nominal conditions); the Primary Heat Exchanger (PHX), which removes 5 MW of heat from the lithium and transfers it to the oil loops; and the Dump Tank, which stores the entire lithium inventory (approximately 14 m^3) during maintenance and shutdown operations. Additionally, part of the Impurity Control System loop is also located within the LLC, including the Nitrogen Trap, positioned near the Dump Tank with a similar lithium capacity, and the cooling system for the C-traps. Figs. 2b and 3 show a scheme of the mentioned components and their location in the room. The remaining rooms are dedicated to Impurity Control Systems, each containing the C-Traps, H-Traps, and Monitoring equipment. Fig. 4a and b and Fig. 5a and b illustrate the layouts of the H-trap and C-Trap rooms, respectively, including the trap locations. A more detailed description of the Lithium

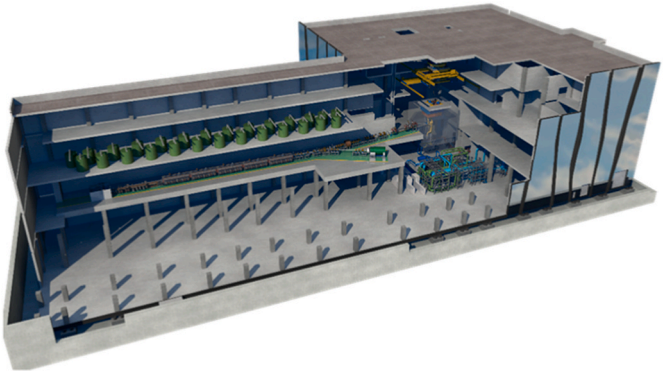

Fig. 1. IFMIF-DONES building.

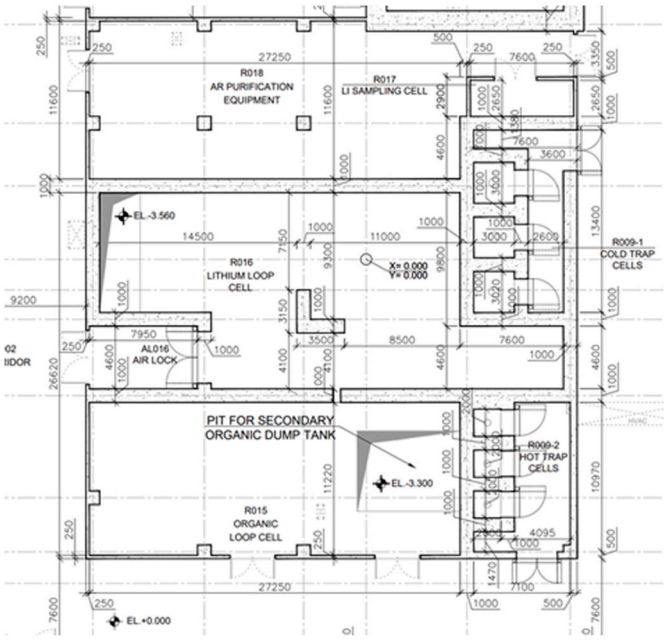

Fig. 2a. Plane of the Lithium System rooms.

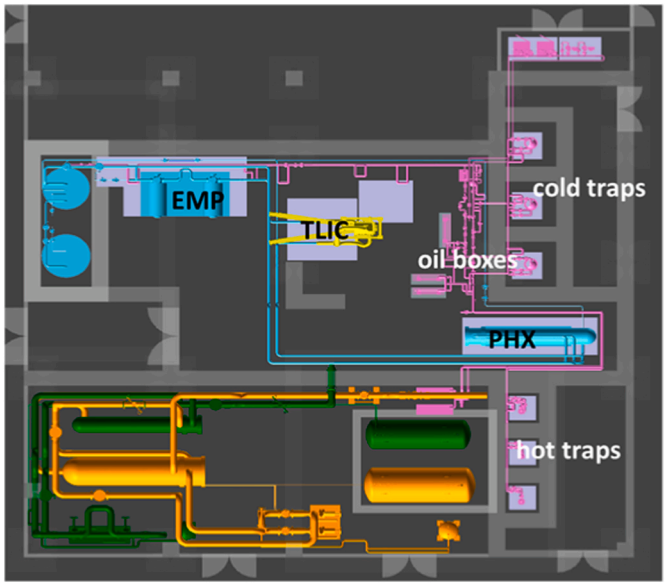

Fig. 2b. Scheme of Lithium system rooms with components.

Systems is provided in Ref. [3].

RAMI (Reliability, Availability, Maintainability and Inspectability) analyses of the Lithium Systems have been conducted due to their critical importance for the reliable and safe operation of the facility, to achieve a high inherent availability of 94 % [4,5]. Lithium leakage represents one of the primary causes of emergency shutdowns, owing to its associated safety and fire risks.

A defense-in-depth methodology has been implemented in IFMIF-DONES [6]. All lithium-related rooms are inertized with an argon (Ar) atmosphere to minimize the risk of fire in case of accidental leakage. They are designed with dynamic confinement, operating under sub-atmospheric pressure. Dedicated argon purification and conditioning systems are incorporated to ensure the required atmospheric quality and temperature within the lithium rooms [7,8]. Those rooms are leak-tight, sealed with a stainless steel liner that acts as a confinement

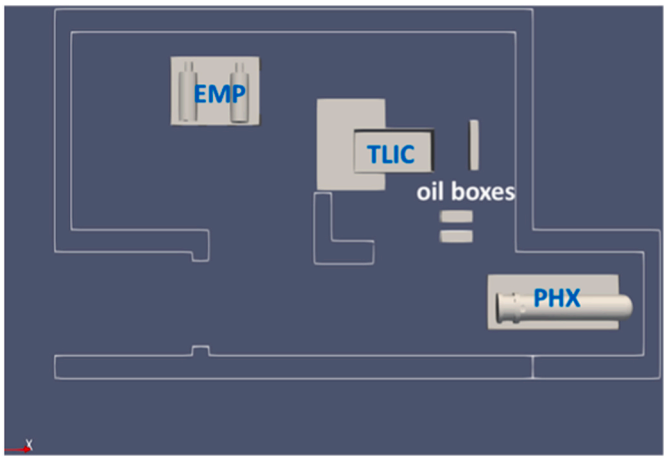

Fig. 3. Scheme of the LLC room and the elements considered in the MCNP model.

barrier.

The lithium rooms are equipped with a dedicated Lithium Recovery System [6], designed to ensure both safety and containment in the event of lithium leakage. Its primary functions are to enable the immediate detection of lithium leaks, allowing for prompt activation of plant safety protocols and rapid drainage of the lithium loop, and to ensure the recovery of spilled lithium. This is achieved through strategically placed catch panels located beneath the main lithium component able to quench the lithium spillage, limiting the atmosphere exposition, and promoting fast solidification and stabilization. Therefore, these catch panels prevent the spread of leaked lithium (sectorization) and help minimize the associated fire risk. This system includes leak detection wires installed at key locations: along piping, welds, joints (beneath thermal insulation), valves, and other critical components, ensuring comprehensive monitoring of potential leakage points.

Additionally, the room liners prevent any potential contact between spilled lithium and the concrete floor, as molten lithium may react with concrete, which serves as an additional protection and collection measure for potential leaks outside of catch panels.

3. Reference accidental scenarios in the lithium system

Four accidental scenarios have been considered within the LLC room. From a conservative perspective, it is assumed that lithium upstream of the rupture point is released due to the pressure gradient. Transient phenomena during emergency situations and drainage processes are not considered. Additionally, lithium adhered to the inner surfaces of the pipes, as well as lithium contained in the dump tank, which is properly shielded, is neglected. In all scenarios, the lithium within the impurity control system is assumed to be isolated.

The first accidental scenario in the LLC room involves the rupture at the lower section of the loop near the electromagnetic pump (EMP). The typical drainage time is on the order of a few minutes, and numerical simulations estimate a lithium discharge time of approximately 1500 s, implying a significant spill. Most of the lithium in the quench tank, EMP, and associated piping would be lost. An estimated volume of 2.3–3 m^3 of lithium is expected to leak and be collected by a catcher panel (dimensions: 5300 mm × 3000 mm × 160 mm) located beneath the pumps. A conservative estimate considers a maximum leaked volume of 3 m^3.

The second accidental scenario involves the rupture of the inlet pipe interface with the Test Cell Lithium System Interface Cell (TLIC),

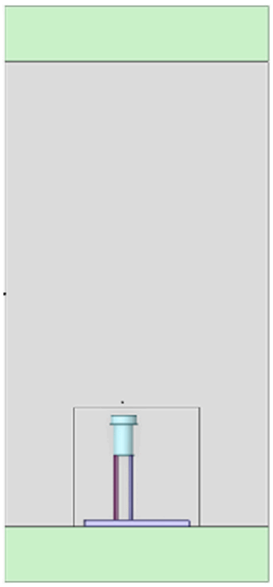

Fig. 4a. Scheme (cross section view) of the H-trap room and elements considered in the MCNP model.

another component in the LLC room containing a significant amount of lithium. In this event, lithium above the rupture point would leak, resulting in the release of approximately 0.66 m^3. This lithium would be collected in a catcher panel (dimensions: 4120 mm × 4120 mm × 160 mm) located directly below the TLIC.

The third accidental scenario in the LLC room is also related to the TLIC and involves the rupture of the outlet pipe interface with TLIC. In this case, most of the lithium in the quench tank would be lost. In the rest of the loop, lithium is likely to be drained as the rupture point is placed at a relatively high position and there are several drainage lines. The estimated leaked volume is about 1.5 m^3.

The fourth accidental scenario in the LLC room considers the rupture of the primary heat exchanger (PHX). It is assumed that most of the lithium within the exchanger would be released and collected in a catcher panel with dimensions 2500 mm × 8000 mm x 220 mm. The leaked volume of leaked lithium in this case is 3.8 m^3.

Two additional components in the Li system should be taken into account in case of an accidental Li leakage: the H-trap and the C-Trap. The concentration of the hydrogen isotopes in the lithium should be kept below specific limits through a system that captures the hydrogen. The capture system is based on a yttrium H-trap which is part of a more general impurity control system where the H-trap is in line with a C-Trap, which can remove other impurities as the oxygen that is a poison for the yttrium. The basic configuration of the H-trap is a set of yttrium pebbles contained inside a stainless-steel mesh crossed by the liquid lithium flow working at the same temperature as the whole loop. The H-trap and C-Trap are located in dedicated rooms. In the event of the H-trap failure, it will be isolated and drainage of lithium in the failed trap will proceed. The estimated Li volume release in such scenario is 0.017 m^3, collected in a catcher panel (1600 mm × 1600 mm x 110 mm) beneath the trap. If the C-Trap fails, approximately 1.074 m^3 of lithium would be released and collected in a panel with dimensions of 1800 mm × 1800 mm × 360 mm.

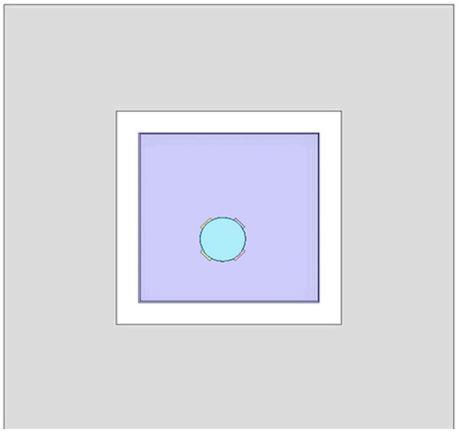

Fig. 4b. Scheme (plant view) of the H-trap room and elements considered in the MCNP model.

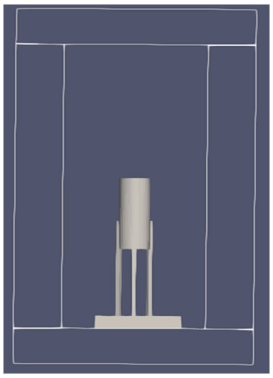

Fig. 5a. Scheme (cross section view) of the C-trap room and elements considered in the MCNP model.

4. Results

4.1. Radiation source terms: ^{7}Be and activation corrosion products

This study considers ^{7}Be and the following ACPs: ^{28}Al, ^{51}Cr, ^{55}Co, ^{56}Co, ^{57}Co, ^{58}Co, ^{60}Co, ^{60m}Co, ^{52}Mn, ^{54}Mn, ^{56}Mn, ^{57}Ni, ^{52}V and ^{181}W.

^{7}Be is dissolved in Li in the form of Be_3N_2. Its concentration inside the H-trap is assumed to be equal to that at the exit of the C-Trap, which depends on both temperature and N content. The temperature at the exit of the C-Trap is 190 °C and the nitrogen concentration in Li is assumed to be 10 wppm, a conservative estimate, given that the baseline nitrogen concentration is assumed to be 30 wppm. Moreover, a 100 % efficiency in the cold trap is assumed. Under these conditions, the ^{7}Be concentration in Li is calculated to be 1.0522×10^{-7} appm (equation 1 in Ref. [9]).

The ACP mass concentrations in Li were derived from a one-dimensional convective mass transfer simulation of the Li loop. The model accounts for mass transfer between the Li flow and the walls of the different components of the Li system, based on local properties such as temperature, material composition, corrosion rates, and flow velocities. ACP transfer is driven by the concentration gradient between the Li and the component surfaces. A convective term is considered for ACP transport along the Li loop. When ACPs reach the test cell they are exposed to irradiation.

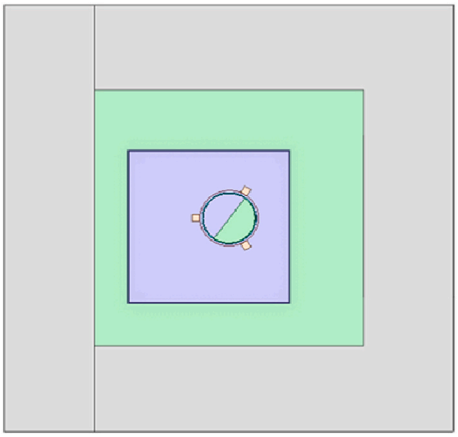

Fig. 5b. Scheme (plant view) of the C-trap room and elements considered in the MCNP model.

To estimate ACP production, activation calculations were performed based on local neutron and deuteron fluxes and the Li volume in each segment of the loop. Since trapping is not explicitly modeled in the simulation, the following assumptions were made to estimate ACP concentration in the H-trap: ACPs with concentrations exceeding their solubility limit at the C-Trap temperature (190 °C) are assumed to be fully trapped (this includes ^{51}Cr, ^{57}Co, and ^{60}Co). In contrast, ^{54}Mn remains below its saturation limit throughout the loop, and thus is unaffected by the C-Trap.

For the activation calculation, the ACP production rates have been computed for the Li segments corresponding to the local neutron and deuteron flux and Li volume. Since the trapping is not modeled explicitly in the convective model next assumptions were considered to estimate ACP concentration in the H-trap: ACPs whose concentration is above the saturated value at C-Trap temperature (190 °C) are completely trapped in the trap (^{55}Fe, ^{51}Cr, ^{57}Co and ^{60}Co). ^{54}Mn does not saturate at loop temperature, hence the C-Trap does not reduce its concentration. Average concentrations of ^{7}Be and the ACPs in the Li loop are presented in Table 1 [10], assuming a Li density of 0.507 g/cm^3. The activity and mass content of ^{7}Be and ACPs released during each accident scenario were calculated based on the volume of Li released, its density, and the concentrations given in Table 1. The corresponding radioactive activities were determined from the mass content and the specific activity of each radionuclide, and are summarized in Table 2.

4.2. Dose assessment in the lithium leakage reference accidental scenarios

^{7}Be and ACPs in lithium are gamma emitters. Ambient dose equivalent, H*(10), per photon was estimated for ^{7}Be and the fourteen ACPs in each of the accidental scenarios using the MCNP 5.1.40 radiation transport code [11]. Ambient dose equivalent, H*(10), is the energy deposited by unit mass by an aligned and expanded radiation field in a point at 10 mm deep in a sphere of 30 cm diameter and 1g/cm^3 density.

Gamma emission energies and intensities were sourced from the JENDL/DDF-2015 nuclear data library [12], and the conversion factors from gamma flux to H*(10) were taken from ICRP Publication 74 [13].

Only those components and devices significantly influencing the transport and scattering of gamma radiation were included in the simulations. In the LLC room, these included: the EMP and the lithium catch panels beneath it, the TLIC and corresponding catch panels, heat exchanger oil boxes, the PHX and its catch panel, as well as the concrete walls, floor, ceiling, and the iron liner covering the walls. In the H-trap

and C-trap rooms, the simulated elements comprised the traps, walls, floor, and ceiling (see Fig. 4a and b and Fig. 5a and b).

In the LLC room, H*(10) per photon was evaluated for each ACP using a 3D rectangular grid covering the entire floor area and extending vertically up to 2 m. The grid resolution was 10 cm × 10 cm × 10 cm. Based on ACP activities and gamma intensities, H*(10) dose rates were calculated for each accidental scenario.

For a rupture at the lower point of the loop (near the EMP), simulation results are shown as dose rate maps at the height of the lithium catch panel (Fig. 6a) and at 2 m above the floor (Fig. 6b). The maximum dose rate at the lithium-contact surface is 85 mSv/h at the initial leakage stage. At a 1-m distance from the source in the source-height plane (1.2 m above the floor), the H*(10) dose rate ranges from 2.5 to 3.4 mSv/h. At 80 cm above the source, the maximum H*(10) rate is 32 mSv/h, while 1 m below it, is 16 mSv/h.

In the scenario involving rupture at the inlet pipe interface with the TLIC, H*(10) rate maps at catch panel level (floor level) and 2 m above the floor are shown in Fig. 7a and b. The maximum dose rate at the source surface is 21 mSv/h. At 1 m distance from the source at floor level, the maximum H*(10) is 0.67 mSv/h, and at 1 m above the source, the maximum estimated H*(10) rate is 7 mSv/h.

H*(10) rate maps are presented in Fig. 8a at floor level and in Fig. 8b at 2 m height above ground for the rupture at the outlet pipe interface with the TLIC. The maximum dose rate, in contact with the source, is 45 mSv/h. In a plane containing the source (floor level), the H*(10) rate at 1 m from the source ranges from 1.16 to 1.28 mSv/h. At 1 m above the ground, the maximum H*(10) rate is approximately 16 mSv/h.

The rupture of the PHX pipe leads to the largest lithium release in the LLC room. Dose rate maps at the lithium catch panel level (floor level) and 2 m height are shown in Fig. 9a and b respectively. The estimated maximum dose rate in contact with the source is 94 mSv/h. At 1 m distance in the source plane, the H*(10) rate ranges between 2.2 and 2.8 mSv/h. At 1 m above the source, the maximum H*(10) rate is around 26 mSv/h.

In the H-trap room, ambient dose equivalent was evaluated in a rectangular box grid covering the whole floor area and extending vertically up to 205 cm in height. In the cold trap room, the grid extended vertically up to 425 cm. In both cases the grid resolution is 5 cm × 5 cm x 5 cm.

For the H-trap leakage scenario, estimated H*(10) rates are shown as dose maps at floor level (Fig. 10a) and 2 m above floor (Fig. 10b), and in a vertical plane perpendicular to the floor through the room center (Fig. 10c). The maximum contact H*(10) rate is 4.2 mSv/h immediately after Li leakage. Maximum H*(10) rate at 1 m above the source is 0.38 mSv/h.

H*(10) rates estimated in the accidental scenario involving lithium leakage out of the C-trap are depicted as dose maps at floor level (Fig. 11a) and 2 m above floor (Fig. 11b) and in a vertical plane through the room center in Fig. 11c. The maximum H*(10) rate, in contact with the catch panel, is 130 mSv/h. At 1 m above the source, the estimated maximum H*(10) rate is 14 mSv/h.

Table 1
ACP concentration in Li (in mg ACP/(kg of Li)).

ACP	mass (mg/kg of Li)
^{54}Mn	8.47×10^{-5}
^{51}Cr	6.90×10^{-9}
^{57}Co	3.22×10^{-4}
^{60}Co	1.71×10^{-5}
^{60m}Co	4.25×10^{-10}
^{55}Co	2.58×10^{-8}
^{56}Co	3.50×10^{-5}
^{58}Co	1.07×10^{-4}
^{52}Mn	2.06×10^{-7}
^{56}Mn	2.14×10^{-8}
^{57}Ni	4.33×10^{-7}
^{181}W	1.61×10^{-12}
^{28}Al	1.38×10^{-10}
^{52}V	1.78×10^{-11}

Table 3 collects for each accidental scenario the Li volume released, the maximum H*(10) rate in contact and the maximum H*(10) rate at 1 m from the source.

Based on the maximum H*(10) dose rates obtained for each reference accidental scenario, the following maximum intervention times are defined to ensure the ICRP-103 occupational maximum annual effective dose limit of 50 mSv is not exceeded [14]. Maximum intervention times are derived by dividing this dose limit by the corresponding maximum H*(10) dose rates in each scenario. The estimated maximum intervention times are conservative as they are based on assuming that the maximum dose rates (in source contact) are received by intervention personnel in each scenario.

However, the 50 mSv/year dose limit is intended for dose accumulation averaged over a full year. The biological effects of radiation exposure can differ significantly between chronic low-dose-rate exposure and acute high-dose-rate exposure, even when the total dose is equivalent. Therefore, the radiological impact of short-term exposures at high dose rates, as modeled in these scenarios, may be more severe than implied by the dose integration alone. This limitation should be considered when planning intervention protocols.

In the event of a rupture at the lower point of the loop near the EMP, human intervention in the room should not exceed 35 min. For a rupture at the inlet pipe interface with the TLIC, the maximum allowable stay time is 143 min. In the case of a rupture at the outlet interface with the TLIC, personnel intervention should be limited to 67 min. If the PHX pipe ruptures, the allowed intervention time is reduced to 32 min. For the reference accident involving Li leakage from the H-trap, the maximum intervention time is 714 min. In the scenario of a C-trap accident, the maximum H*(10) dose rate reaches 130 mSv/h, exceeding the threshold for red zone classification (>100 mSv/h). Consequently, human access is prohibited, and remote handling systems must be implemented.

Regarding the temporal evolution of the H*(10) rate following the lithium leakage, one week after the incident, the H*(10) rate drops to approximately 70 % of its initial value. After two weeks, it further decreases to about 65 %, and after one month, it reaches 57 %. Three months post-leakage, the dose rate is 36 % of the initial value, and after 6.5 months, it falls to just 17 %. Following the first week, once the short-lived activation products (ACPs) have decayed and no longer contribute significantly to the dose, the H*(10) rate follows approximately an exponential decay. The fraction of initial maximum dose (in %) is represented as a function of time passed after the leakage in Fig. 12.

The contribution of ACPs to the radiation dose at different times after the leakage is presented in Table 4. Among the ACPs, **^{56}Co and ^{58}Co** contribute the most to the dose, accounting for **62 %** of the total dose immediately after the leakage. **^{57}Ni, ^{56}Mn, and ^{28}Al** together contribute approximately **23 %** at this initial stage. However, due to their short half-lives, their contribution becomes negligible in the days that follow. **^{54}Mn and ^{57}Co** make up the remaining **11 %** at the onset of the leakage. The combined contribution of **^{56}Co and ^{58}Co** reaches its peak (**83 %**) two weeks after the leakage. Meanwhile, the combined contribution of **^{54}Mn and ^{57}Co** gradually increases, eventually matching that of **^{56}Co and ^{58}Co** around **36 weeks (8.3 months)** post-accident, with both groups contributing approximately **48 %** to the dose at that time. One year after the leakage **^{54}Mn and ^{57}Co contribute 65 % of the dose, more than double the 30 % contribution of ^{56}Co and ^{58}Co (30 %).**

5. Discussion and conclusion

This study provides a comprehensive radiological assessment of potential lithium leakage scenarios within the IFMIF-DONES lithium system, focusing on the Lithium Test Cell (LLC), Hot Trap, and Cold Trap rooms. The evaluation considered worst-case leakages from critical

Table 2
ACP activities (in Bq) in the Li at the initial stage of the leakage accidental scenarios.

ACP	EMP	TLIC inlet	TLIC outlet	PHX	C-Trap	H-Trap
^{54}Mn	3.69×10^{10}	8.11×10^{9}	1.84×10^{10}	4.67×10^{10}	1.32×10^{10}	2.09×10^{8}
^{51}Cr	3.59×10^{7}	7.89×10^{6}	1.79×10^{7}	4.54×10^{7}	1.28×10^{7}	2.03×10^{5}
^{57}Co	1.53×10^{11}	3.36×10^{10}	7.63×10^{10}	1.93×10^{11}	5.46×10^{10}	8.65×10^{8}
^{60}Co	1.09×10^{9}	2.39×10^{8}	5.43×10^{8}	1.38×10^{9}	3.89×10^{8}	6.16×10^{6}
^{55}Co	4.71×10^{9}	1.04×10^{9}	2.36×10^{9}	5.97×10^{9}	1.69×10^{9}	2.67×10^{7}
^{56}Co	5.94×10^{10}	1.31×10^{10}	2.97×10^{10}	7.52×10^{10}	2.13×10^{10}	3.37×10^{8}
^{58}Co	1.91×10^{11}	4.21×10^{10}	9.56×10^{10}	2.42×10^{11}	6.84×10^{10}	1.08×10^{9}
^{52}Mn	5.20×10^{9}	1.14×10^{9}	2.60×10^{9}	6.59×10^{9}	1.86×10^{9}	2.95×10^{7}
^{56}Mn	2.61×10^{10}	5.74×10^{9}	1.30×10^{10}	3.31×10^{10}	9.34×10^{9}	1.48×10^{8}
^{57}Ni	3.76×10^{10}	8.27×10^{9}	1.88×10^{10}	4.76×10^{10}	1.35×10^{10}	2.13×10^{8}
^{181}W	5.39×10^{2}	1.19×10^{2}	2.70×10^{2}	6.83×10^{2}	1.93×10^{2}	3.06
^{28}Al	2.32×10^{10}	5.10×10^{9}	1.16×10^{10}	2.94×10^{10}	8.31×10^{9}	1.31×10^{8}
^{60m}Co	7.15×10^{9}	1.57×10^{9}	3.58×10^{9}	9.06×10^{9}	2.56×10^{9}	4.05×10^{7}
^{52}V	9.67×10^{8}	2.13×10^{8}	4.83×10^{8}	1.22×10^{9}	3.46×10^{8}	5.48×10^{6}
^{7}Be	2.08×10^{3}	4.58×10^{2}	1.04×10^{3}	2.64×10^{3}	7.45×10^{2}	1.18×10^{1}

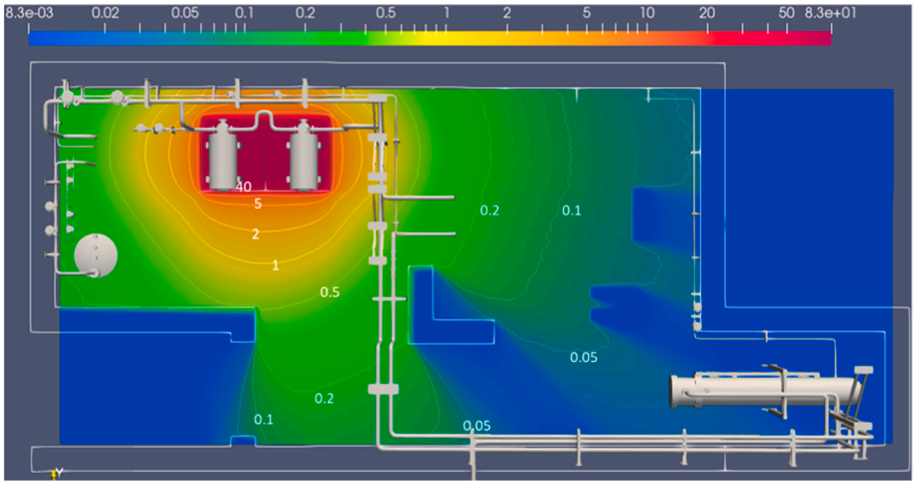

Fig. 6a. H*(10) rate (mSv/h) in the LLC room at source level in case of rupture of lower point of the loop close to the electromagnetic pump.

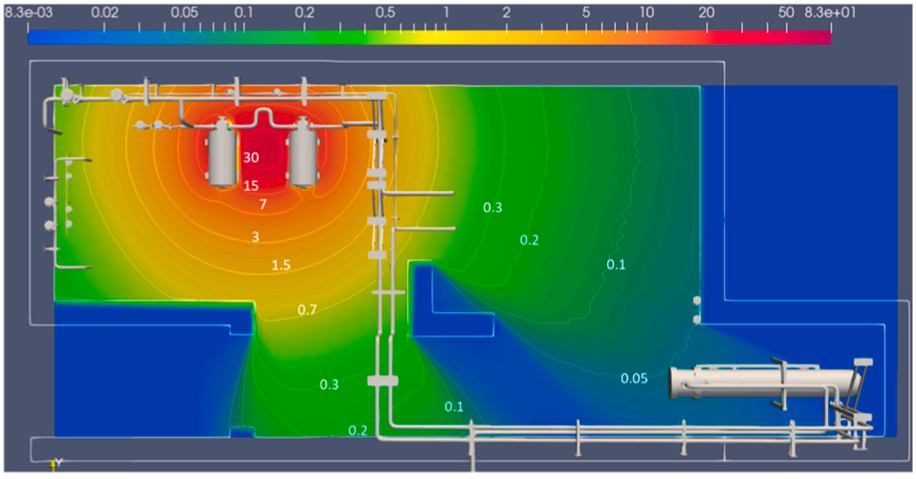

Fig. 6b. H*(10) rate (mSv/h) in the LLC room 2 m above the floor in case of rupture of lower point of the loop close to the electromagnetic pump.

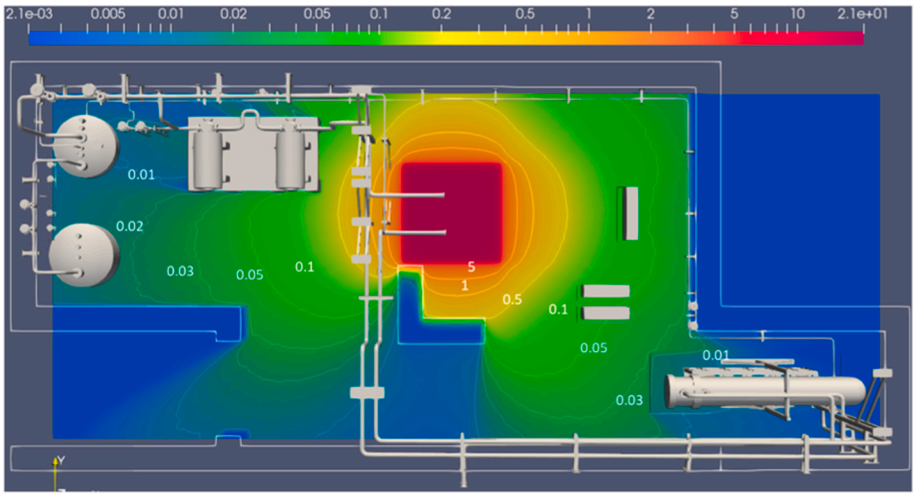

Fig. 7a. H*(10) rate (mSv/h) in the LLC room at floor level in case of rupture of inlet pipe interface of TLIC.

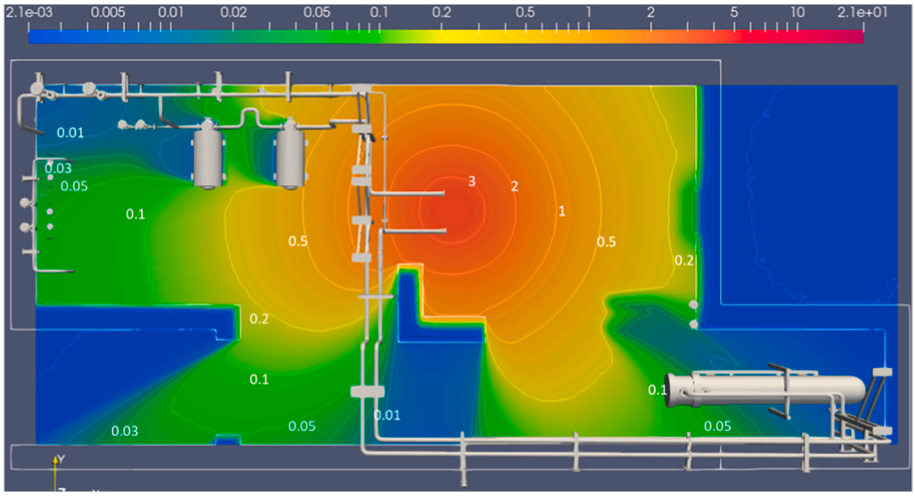

Fig. 7b. H*(10) rate (mSv/h) in the LLC room 2 m above the floor in case of rupture of inlet pipe interface of TLIC.

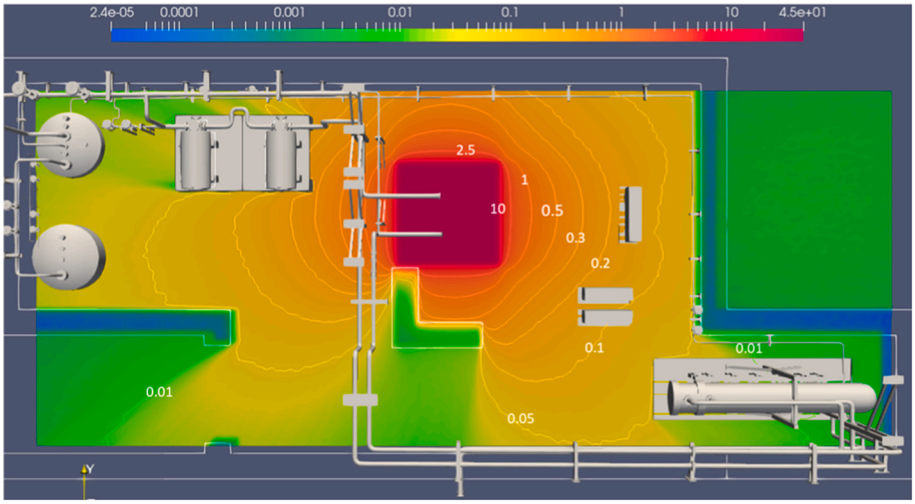

Fig. 8a. H*(10) rate (mSv/h) in the LLC room at floor level in the rupture of outlet pipe interface of TLIC.

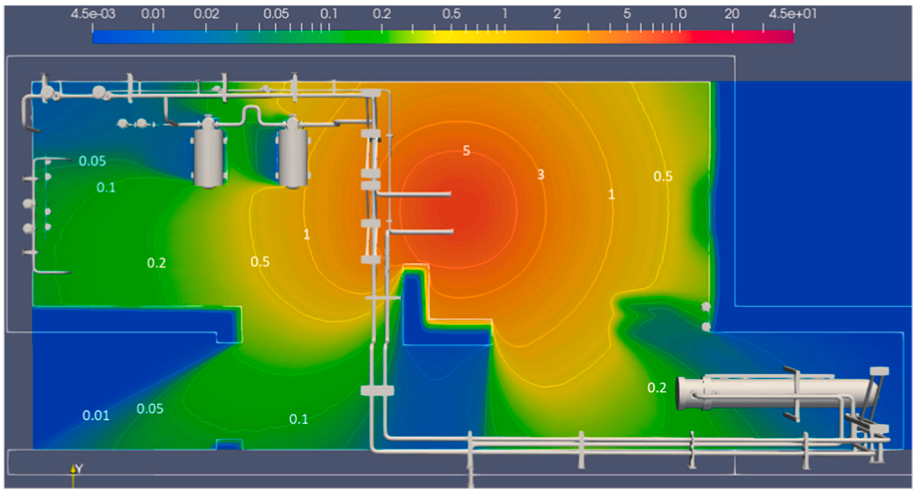

Fig. 8b. H*(10) rate (mSv/h) in the LLC room 2 m above the floor in the rupture of outlet pipe interface of TLIC.

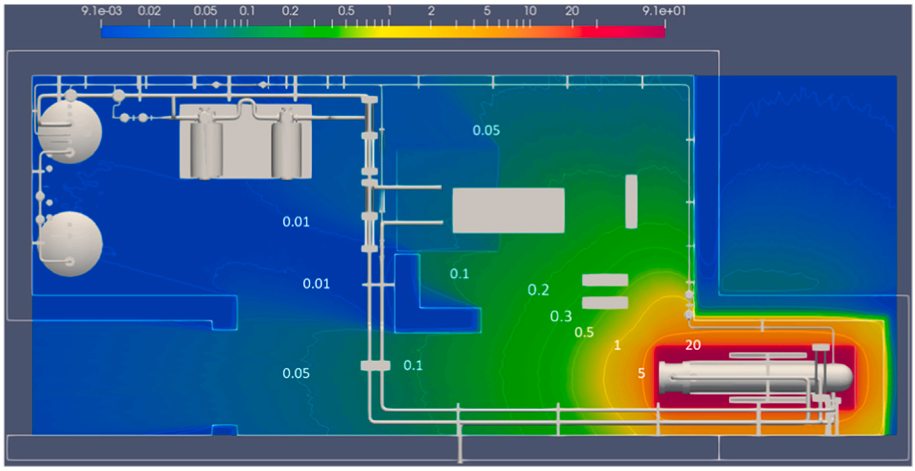

Fig. 9a. H*(10) rate in the LLC room at floor level immediately after rupture of PHX pipe.

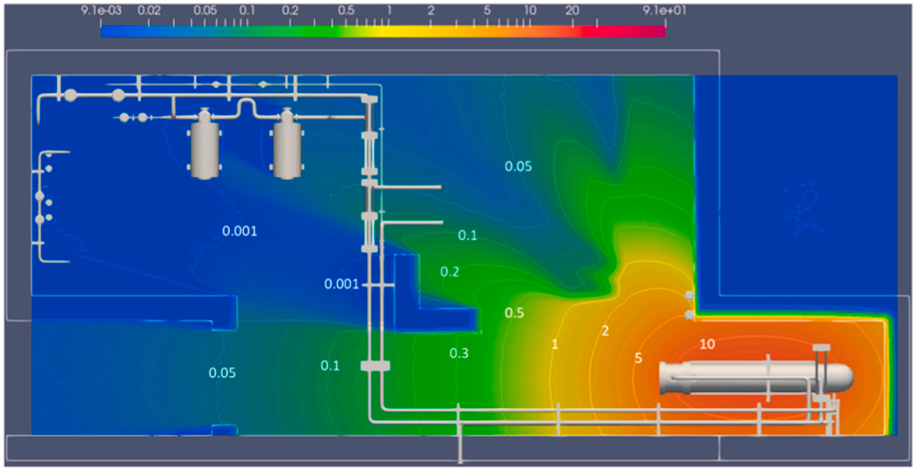

Fig. 9b. H*(10) rate in the LLC room 2 m above floor in the rupture of PHX pipe.

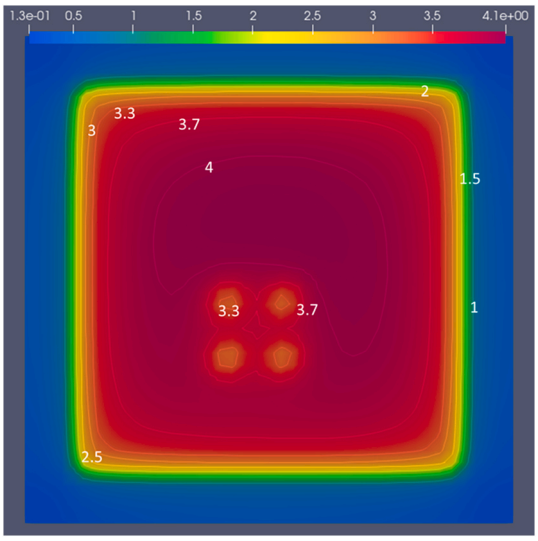

Fig. 10a. H*(10) rate (mSv/h) in the H-trap room in a plane at floor height in the H-trap Li leakage scenario.

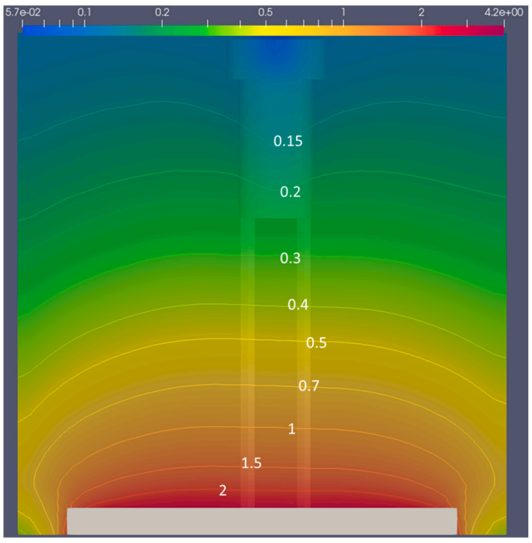

Fig. 10c. H*(10) rate (mSv/h) in the H-trap room in a plane perpendicular at ground passing through the middle of the room in the H-trap rupture scenario.

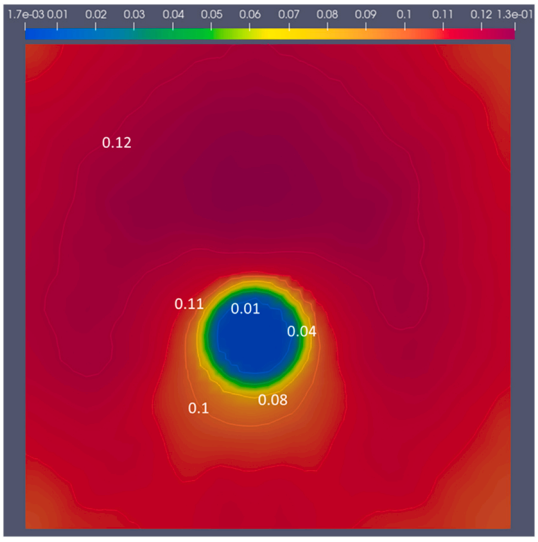

Fig. 10b. H*(10) rate (mSv/h) in the H-trap room in a plane 2 m above floor in the H-trap Li leakage scenario.

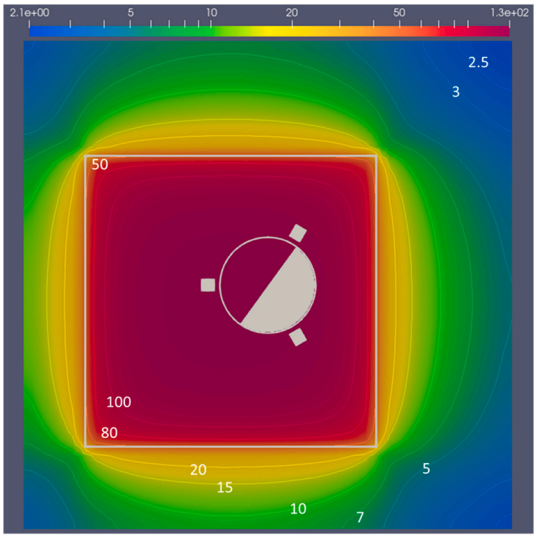

Fig. 11a. H*(10) rate (mSv/h) in the C-trap room in a plane at floor height in the C-trap Li leakage scenario.

components, estimating lithium volumes, their distribution in containment systems, and the associated ambient dose equivalent rates, H*(10), due to activated corrosion products (ACPs) and ^{7}Be.

The scenarios in the LLC room demonstrate that lithium discharge events from major components, particularly the EMP, TLIC interfaces, and the PHX, pose significant radiological risks due to both the volume of released lithium and the resulting gamma dose rates. The PHX rupture was found to generate the highest immediate H*(10) contact dose rate (94 mSv/h), closely followed by the EMP rupture scenario (85 mSv/h), both exceeding standard thresholds for personnel intervention. These conditions necessitate strict access controls and time-limited interventions to remain within the annual 50 mSv occupational dose limit.

Scenarios involving TLIC interfaces presented comparatively lower dose rates but still required access limitations. The inlet and outlet TLIC pipe ruptures resulted in maximum surface dose rates of 21 mSv/h and 45 mSv/h respectively, necessitating intervention times of less than 2.5 h.

In the H-Trap and C-Trap rooms, although the volume of lithium released is substantially lower, the Cold Trap rupture posed an exceptional radiological hazard. The estimated contact dose rate of 130 mSv/h categorizes the area as a red zone, thus mandating remote handling and complete restriction of human access post-accident.

Regarding the contribution of individual radionuclides, the study shows that ^{56}Co and ^{58}Co dominate the dose contribution immediately post-accident, while the longer-lived ^{54}Mn and ^{57}Co become the primary contributors at later stages. The time-dependent dose profile underlines the importance of radionuclide-specific decay analyses when planning emergency responses and maintenance schedules.

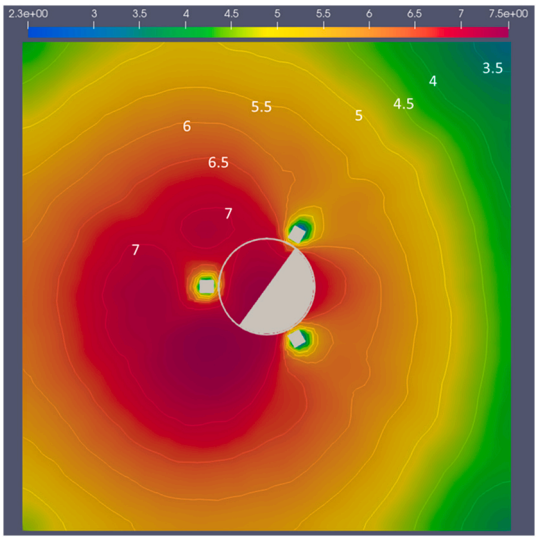

Fig. 11b. H*(10) rate (mSv/h) in the C-trap room in a plane 2 m above floor in the C-trap Li leakage scenario.

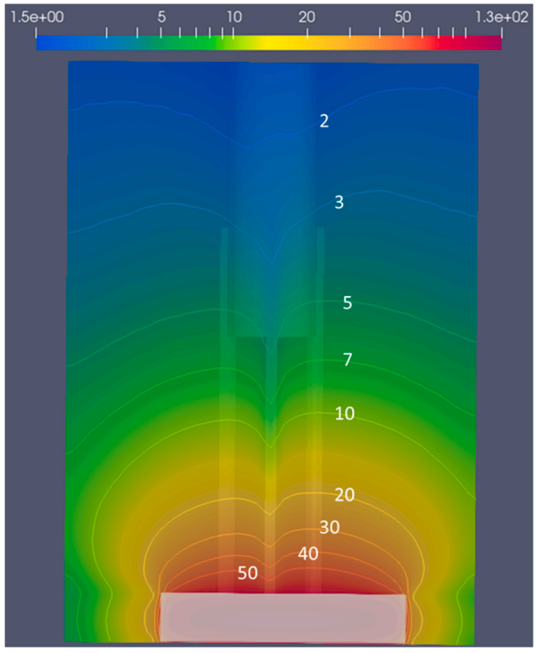

Fig. 11c. H*(10) rate (mSv/h) in the C-trap room in a plane perpendicular at ground passing through the middle of the room in the C-trap Li leakage scenario.

In conclusion, the results highlight the need for strategic placement and sizing of lithium catchment systems to minimize spread and maximize shielding effectiveness, remote handling systems especially in areas prone to high-dose rates (e.g., C-Trap room), time-restricted human access post-leakage, guided by real-time dosimetry and radionuclide decay modeling, robust isolation and drainage protocols for critical components to mitigate the radiological impact of failures.

The insights gained from this study are essential for improving accident response strategies and enhancing the overall safety design of the IFMIF-DONES lithium system. Future work could expand to consider dynamic drainage modeling, heat transfer effects, and coupled mechanical-radiological failure analysis to further refine safety protocols.

Table 3
Maximum H*(10) rate in contact with the source and at 1 m of the source, and released Li volumes in each accidental scenario.

scenario	Li volume m^3	H*(10) contact mSv/h	H*(10), 1 m mSv/h
EMP rupture	3	85	30
TLIC inlet pipe rupture	0.66	21	7
TLIC oulet pipe rupture	1.5	45	16
PHX rupture	3.8	94	26
H-trap rupture	0.017	4.2	0.38
C-trap rupture	1.074	130	14

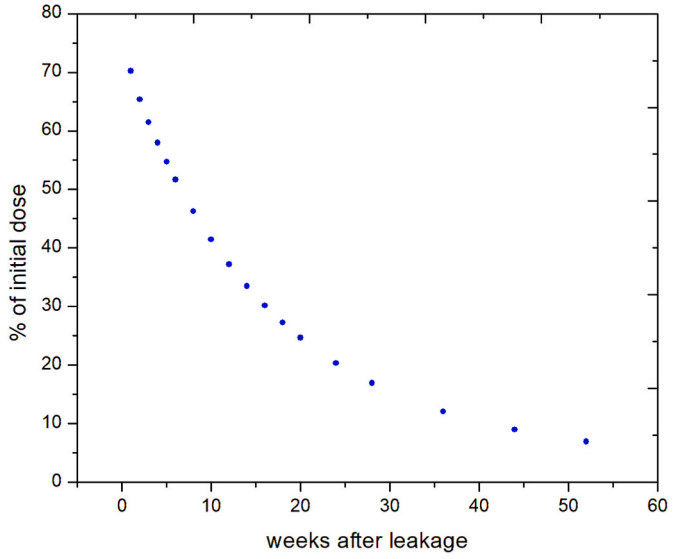

Fig. 12. Fraction of initial dose (in %) as a function of time passed after lithium leakage.

CRediT authorship contribution statement

J. Javier Martínez-Serrano: Writing – original draft, Software, Methodology, Investigation, Conceptualization. **Jorge Maestre:** Writing – review & editing, Methodology, Conceptualization. **Yuefeng Qiu:** Writing – review & editing, Supervision, Methodology. **Francesco Saverio Nitti:** Writing – review & editing, Supervision.

Declaration of competing interest

The authors declare that they have no known competing financial interests or personal relationships that could have appeared to influence the work reported in this paper.

Table 4
ACP contribution (in %) to dose along time passed after the leakage.

Time (weeks)	$^{56}Co + {}^{58}Co$	$^{54}Mn + {}^{57}Co$	$^{57}Ni + {}^{56}Mn + {}^{28}Al$	^{60}Co
Initial	61.8	10.7	23	0.5
1	82.4	15.0	0.5	0.7
2	83.0	15.9	0.02	0.7
3	82.7	16.6	0	0.7
4	82.1	17.3	0	0.8
5	81.5	18.1	0	0.8
6	80.7	18.8	0	0.9
8	79.2	20.3	0	1.0
10	77.5	22.0	0	1.1
12	75.7	23.7	0	1.2
14	73.8	25.5	0	1.3
16	71.9	27.4	0	1.5
18	69.8	29.3	0	1.6
20	67.7	31.4	0	1.8
24	63.2	35.7	0	2.1
28	58.5	40.2	0	2.5
36	48.7	48.2	0	3.5
44	38.9	56.8	0	4.6
52	30.0	64.5	0	5.9

Acknowledgements

We are grateful to Fernando Mota (CIEMAT, Spain) for his valuable guidance and assistance with SpaceClaim, SuperMC, and ParaView software tools.

References

[1] W. Królas, A. Ibarra, F. Arbeiter, F. Arranz, D. Bernardi, M. Cappelli, J. Castellanos, T. Dézsi, H. Dzitko, P. Favuzza, A. García, J. Gutiérrez, M. Lewitowicz, A. Maj, F. Martin-Fuertes, G. Micciché, A. Muñoz, F.S. Nitti, T. Pinna, I. Podadera, J. Pons, Y. Qiu, R. Román, M. Toth, A. Zsakai, The IFMIF-DONES fusion oriented neutron source: evolution of the design, Nucl. Fusion 61 (12) (2021) 125002.

[2] F. Martín-Fuertes, M.E. García, P. Fernández, A. Cortés, G. D'Ovidio, E. Fernández, T. Pinna, M.T. Porfiri, U. Fischer, F. Ogando, F. Mota, Y. Qiu, A. Helminen, S. Potempski, E. Gallego, A. Ibarra, Integration of safety in IFMIF-DONES design, Saf. Now 5 (4) (2019).

[3] F.S. Nitti, J. Maestre, T. Dezsi, S. Gordeev, N. Holstein, B. Brenneis, L. Buligins, J. Molla, A. Ibarra, The lithium systems of the IFMIF-DONES facility, Nucl. Fusion (2025), https://doi.org/10.1088/1741-4326/adc284. Accepted Manuscript.

[4] T. Pinna, D.N. Dongiovanni, K. Kowal, J. Kałowski, S. Potempski, D. Rechena, J. J. Rueda, RAMI studies for DONES, Nucl. Fusion (2025), https://doi.org/10.1088/1741-4326/adc7ca. Accepted Manuscript.

[5] J.J. Rueda, D.N. Dongiovanni, T. Pinna, C. Torregrosa-Martin, A. Ibarra, J. Maestre, F.S. Nitti, RAMI analysis of DONES lithium systems updated to the last design modifications, Fusion Eng. Des. 193 (2023) 113792.

[6] G. D'Ovidio, F. Martín-Fuertes, J.C. Marugán, S. Bermejo, F.S. Nitti, Lithium fire protection design approach in IFMIF-DONES facility, Fusion Eng. Des. 189 (2023) 113446.

[7] A. Manjavacas, M.A. Vázquez-Barroso, C. Torregrosa-Martín, J. Maestre, F. Martín-Fuertes, Definition and optimization of a MELCOR model of the IFMIF-DONES argon purification subsystem, Fusion Eng. Des. 205 (2024) 114560.

[8] K. Kowal, Failure mode and reliability study for dynamic confinement and conditioning of the IFMIF-DONES radiological areas, Fusion Eng. Des. 186 (2023) 113342.

[9] M. Ida, Estimation and control of beryllium-7 behavior in liquid lithium loop of IFMIF, Fusion Eng. Des. 82 (2007) 2490–2496.

[10] J. Martinez-Serrano, Y. Qiu, T. Dezsi, F.S. Nitti, A. Ibarra, Radiation dose assessment of 7Be and activated corrosion products present in the hydrogen trap of IFMIF-DONES lithium system, Fusion Eng. Des. 201 (2024) 114269.

[11] J.E. Sweezy, T.E. Booth, F.B. Brown, J.S. Bull, R.A. Forster III, J.T. Goorley, H. G. Hughes III, R.L. Martz, R.E. Prael, A. Sood, A.J. Zukaitis, R.C. Little, H.R. Trellue, M.C. White, M.B. Lee, S.M. Girard, MCNP - a General Monte Carlo N-Particle Transport Code, Version 5 - Volume 1: Overview and Theory, Los Alamos National Laboratory Tech. Rep. LA-UR-03-1987, 2003.

[12] J. Katakura, F. Minato, "JENDL Decay Data File 2015" "JAEA-Data/Code 2015-030, 2016.

[13] ICRP, Conversion coefficients for use in radiological protection against external radiation, ICRP publication 74, Ann. ICRP 26 (1996) 3–4.

[14] ICRP, in: The 2007 Recommendations of the International Commission on Radiological Protection, vol. 37, ICRP Publication 103. Ann. ICRP, 2007, pp. 2–4.